Morphology and Mechanical Properties of Interpenetrating Polymer Networks of Poly(allyl diglycol carbonate) and Rigid Polyurethane

SUSAN DADBIN,[1] R. P. CHAPLIN[2]

[1] Radiation Processing Center, Atomic Energy Organization of Iran, P.O. Box 14155–4494, Tehran, Iran

[2] University of New South Wales, Sydney 2052, Australia

Received 15 June 2000; accepted 28 August 2000

ABSTRACT: Novel simultaneous interpenetrating polymer networks (SINs) of poly(allyl diglycol carbonate) (ADC) and a rigid high modulus polyurethane based on the Conathane UC-33 prepolymer system (UC) were synthesized. The completion of each component reaction was verified by means of Fourier transform IR spectroscopy. The effects of the composition on the morphology, mechanical properties, and thermal transition behavior of the SINs were studied. At 10% composition, transmission electron microscopy revealed complete phase miscibility. This was also supported by the high optical transparency of the sample. As the UC content increased to 20% a two-phase morphology was observed in which the UC phase domains were dispersed in the matrix of the ADC phase. At higher UC content the ADC continuous phase was replaced by the UC phase, implying the occurrence of phase inversion. This variation of morphology allowed the SINs to have a property range from the UC-toughened plastics to the ADC-reinforced polyurethane. The SINs containing 50% UC showed synergism in the mechanical properties as the elongation was significantly increased to 4 times that of the unmodified UC and ADC homopolymers. © 2001 John Wiley & Sons, Inc. J Appl Polym Sci 81: 3361–3370, 2001

Key words: simultaneous interpenetrating polymer networks; poly(allyl diglycol carbonate); rigid polyurethane; morphology; fracture properties

INTRODUCTION

Interpenetrating polymer networks (IPNs) are one on the fastest growing fields in multicomponent polymer materials. They are defined as a combination of two or more polymers in a network form in which at least one of them is synthesized and/or crosslinked in the immediate presence of the other.[1–3] Among the different methods of formation of IPNs, simultaneous IPNs (SINs) have received more attention because of their ease of synthesis and the ability to control their morphology with several factors.[4,5] Because the morphology of multiphase materials significantly affects their properties, the formation of SINs is a new approach for combining the polymer components to achieve the desired properties.

The degree of intermixing of SINs is mainly affected by the thermodynamic miscibility of the components,[6,7] the relative rate of network formation,[8–10] the composition,[11,12] the degree of crosslinking, and the mobility of the polymer chains at the time of phase separation.[11,13,14] However, complete miscibility is not essential to achieve complete phase mixing, because the permanent entanglements and crosslinking associated with simultaneous polymerization restricts phase separation.[15,16] Maximum restriction of

Correspondence to: S. Dabin (sdabin@seai.neda.net.ir).

Journal of Applied Polymer Science, Vol. 81, 3361–3370 (2001)

Table I Materials Used in Preparation of IPNs

Materials	Description	Source
Conathane UC-33		
Part A (prepolymer)	Based on dicyclohexylmethane-4,4′-diisocyanate	Conap, Inc.
Part B (prepolymer)	Based on phenylmercuric oleate and ethohexadiol	Conap, Inc.
Allylic monomer	Allyl diglycol carbonate	SOLA, Inc.
Initiator	Benzoyl peroxide	Interox

phase separation should result when the polymer begins to gel near or before phase separation of the two components. If phase separation precedes gelation, the domains are relatively large and the crosslinking stabilizes the phase-separated morphology.[16]

Most IPNs involve heterogeneous systems that have one elastomeric phase and one glassy phase. This combination of elastomeric and glassy networks often allows IPNs to range in properties from filler-reinforced elastomers to rubber-toughened plastics, depending on which component becomes the continuous phase.[8] Some attempts have been made to improve the fracture toughness of glassy polymers through formation of a variety of IPNs.[10,11,17–20] However, increasing the fracture toughness of the glassy network is usually accompanied by a significant reduction in the modulus and tensile strength values of the IPN system. Increasing the modulus of the elastomeric component improves the tensile strength and modulus values of the IPNs.[11,17] In the present work we introduce novel SINs based on poly(allyl diglycol carbonate) (ADC) and a rigid, high glass-transition temperature (T_g) polyurethane based on the Conathane UC-33 prepolymer system (UC). The effects of the SIN composition on the morphology and mechanical properties of the ADC/UC SINs were investigated by transmission electron microscopy (TEM), dynamic mechanical analysis (DMA), scanning electron microscopy (SEM), conventional tensile testing, and single edge notch tension fracture toughness methods. The toughening mechanisms of the SINs were also discussed.

EXPERIMENTAL

Materials

The raw materials used for the ADC/UC SINs and their descriptions are listed in Table I. They were used without further purification.

Synthesis

Casting of ADC Homopolymer

Dried benzoyl peroxide powder as the radical initiator (3% w/w) was dissolved in ADC monomer with vigorous stirring at 50°C. The solution was degassed and then poured into a glass mold and polymerized as flat 3 mm thick sheets in a temperature-programmed oven. The temperature was slowly increased from 50 to 85°C over a period of 22 h. The ADC samples were then removed from the mold and postcured at 105°C for 2 h.

Casting of SINs

The isocyanate terminated polyurethane prepolymer (part A) and its curing agent (part B) in appropriate proportions were mixed with ADC monomer containing 3% (w/w) initiator and stirred thoroughly to form a clear solution. The mixture was then degassed to remove dissolved gas, and then it was introduced into the glass mold and polymerized using the same method as the ADC homopolymer. The SINs were postcured at 105°C for 2 h. The completion of each component reaction was verified by the disappearance of the absorbance of the NCO peak at 2270 cm^{-1} and the allyl peak at 3092 cm^{-1} using a Perkin–Elmer 2000 Fourier transform IR (FTIR) spectrometer. A typical FTIR spectrum of the ADC/UC SINs is shown in Figure 1.

Casting of Polyurethane

The isocyanate terminated polyurethane prepolymer (part A) was mixed with the curing agent (part B) in appropriate proportions and thoroughly stirred. The mixture was degassed for about 10 min to remove the entrapped air caused by mixing and immediately poured into the mold. The sample was cured for 24 h at 65°C and then postcured at 105°C for 2 h.

Stress–Strain

The stress–strain properties were determined on an Instron testing machine (model 1115). The

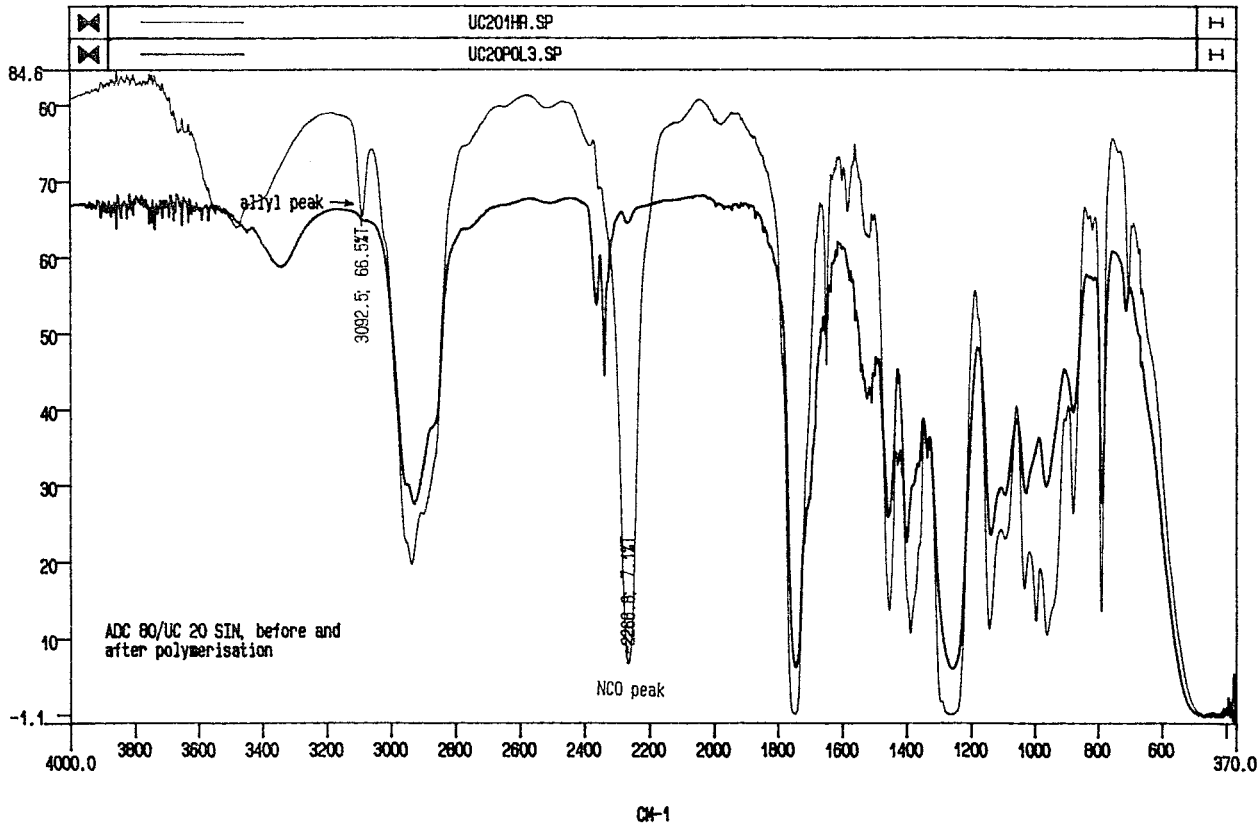

Figure 1 FTIR spectra of the ADC80/UC20 SIN before and after polymerization.

specimens had dimensions of 120 × 12 × 3 mm. The test procedure was carried out at a crosshead speed of 1 mm/min at 22°C using flat-faced grips at an intergrip distance of 60 mm.

Single Edge Notched Tension

Molded sheets of samples were cut into specimens with dimensions of 120 × 15 × 3.4 mm. The fracture toughness or stress intensity at the onset of crack propagation (K_{1c}) was measured at a crosshead speed of 1 mm/min at 22°C according to the following equation[21]:

$$Y = K_{1c}BW/Pa^{1/2} = 1.99 - 0.41(a/W) + 18.70(a/W)^2 - 38.48(a/W)^3 + 53.85(a/W)^4$$

where a is the crack length, W is the width of the specimen, B is the thickness of the specimen, and P is the applied load.

Thermal Transition

The thermal transition behaviors of the SINs and homopolymers were determined using a DuPont dynamic mechanical analyzer (model 983) in resonance mode. The loss modulus maximum was taken as the glass-transition temperature.

TEM Observation

A small piece of each SIN sample was stained in 2% aqueous osmium tetroxide vapors for 1 week. The samples were trimmed and then thin sectioned (80 nm) with a Reichert–Jung Ultra Cut E ultramicrotome. The electron micrographs were observed in a Hitachi electron microscope (H-7000). The polyurethane phase was stained with osmium tetroxide and appeared as the darker area in the TEM micrographs.

Image Analysis

The image analysis was performed using selected TEM micrographs with a Quantimet 500 image analyzer (Leica Cambridge Ltd.) that provided the particle size analysis.

SEM Study

The fracture surfaces of the samples were studied by SEM using a Cambridge Stereoscan 360. Small pieces of the fractured samples were cut and

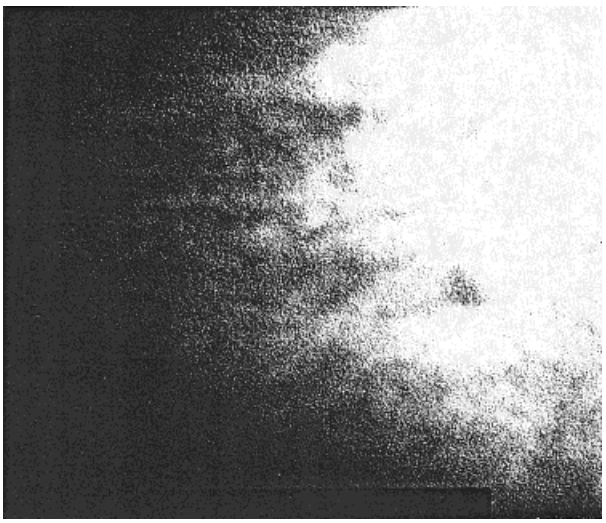

Figure 2 A TEM micrograph of the ADC90/UC10 SIN (original magnification ×100,0000).

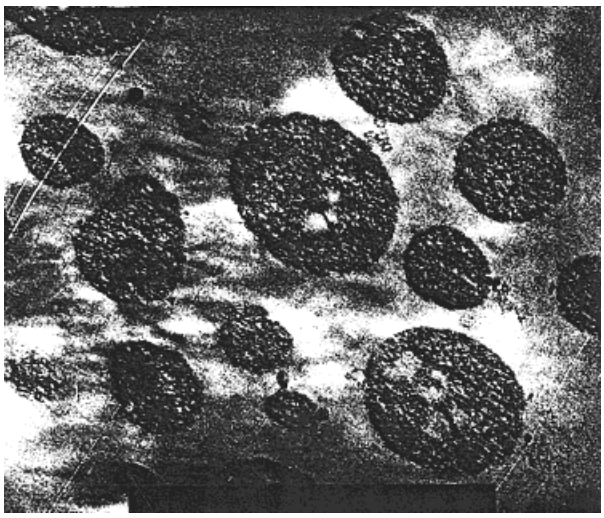

Figure 3 A TEM micrograph of the ADC80/UC20 SIN (original magnification ×2500).

mounted on aluminum stubs with silver paint adhesives. The samples were coated with gold by a Polaron SEM sputter coater with a magnetron head and then observed on a SEM 360.

RESULTS AND DISCUSSION

Morphology

The TEM micrographs of the ADC90/UC10 SIN showed no apparent phase domains, even at a magnification of 100,000 (Fig. 2), indicating complete phase mixing. The single phase morphology of the ADC90/UC10 SIN was also supported by the high optical transparency of the sample. A two-phase morphology was obtained by increasing the UC content to 20% in which the UC phase domains were dispersed in the matrix of the ADC resin as shown in Figure 3. The dispersed phase domain sizes ranged from 1.2 to 10 μm as measured by the image analysis technique. The UC domains contained very small occlusions of the ADC phase. It seemed that the ADC subdomains captured within the UC domains were the polymerization products of the ADC monomer, which could not diffuse out of the UC phase because of the high viscosity of the medium. In fact the faster gel formation of the polyurethane at a UC content of 20% (compared to 10%) produced polyurethane microgels that were swollen with ADC monomer. Then the trapped ADC in the polyurethane microgels formed a separate phase after polymerization that was due to their thermodynamic immiscibility.

A different morphology was observed at 30% UC content where the ADC continuous phase was replaced by the UC phase, which implied the occurrence of phase inversion (Fig. 4). The dispersed ADC particles within the UC matrix phase in this sample were characterized by a bimodal size distribution with large particle sizes (3–12 μm) and small particle sizes (0.1–0.9 μm). A typical particle size distribution for smaller ADC particles determined by the image analysis technique is shown in Figure 5. The bimodal particle size distribution was retained as the UC content increased to 50% (Fig. 6), but the ADC domain size range decreased to 0.9–4 μm for large parti-

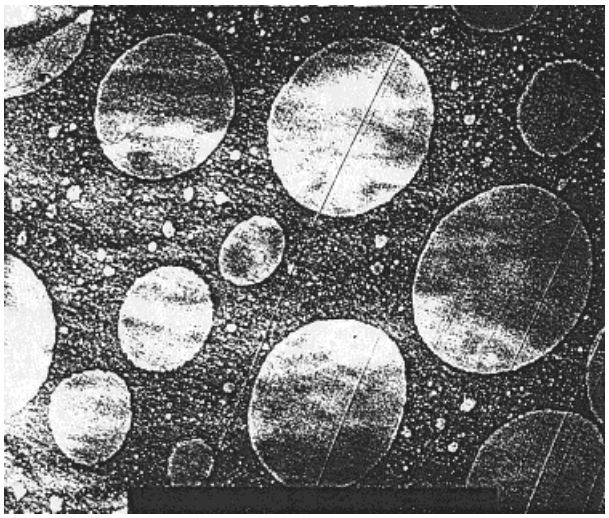

Figure 4 A TEM micrograph of the ADC70/UC30 SIN (original magnification ×2500).

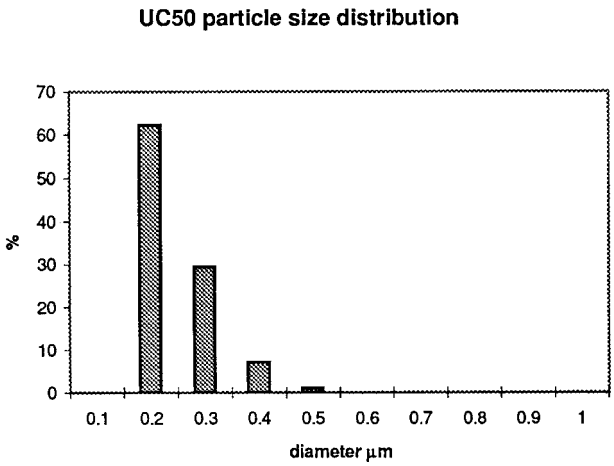

Figure 5 The equivalent spherical diameter distribution of the small particles range of the ADC70/UC30 SIN.

cles and to 0.03–0.1 μm for small particles. This decrease in the particle size of the ADC domains with increasing UC content from 30 to 50% was an expected result, because the UC phase at these compositions was a matrix phase and one could expect that the decrease in the ADC phase content would lead to the formation of smaller phase domains. It was interesting that some of the ADC particles in Figure 6 showed a distinct circumferential region that is clearly shown in Figure 7 at higher magnification. This may show the interfacial zone between the UC matrix phase and the ADC dispersed phase. The fracture surface studies of this sample also confirmed the strong phase intermixing at the phase boundaries.

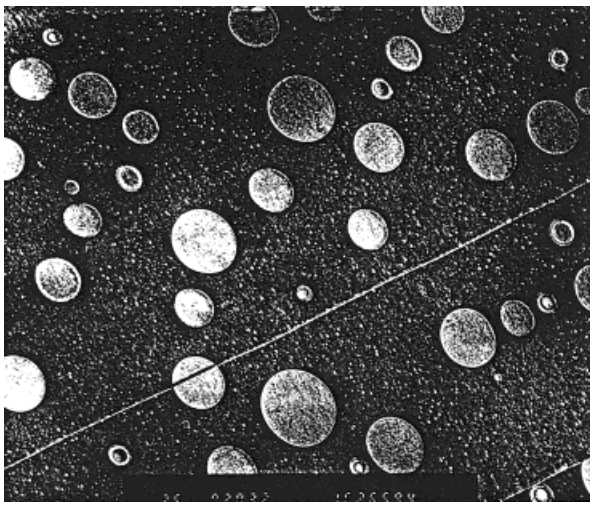

Figure 6 A TEM micrograph of the ADC 50/UC50 SIN (original magnification ×2500).

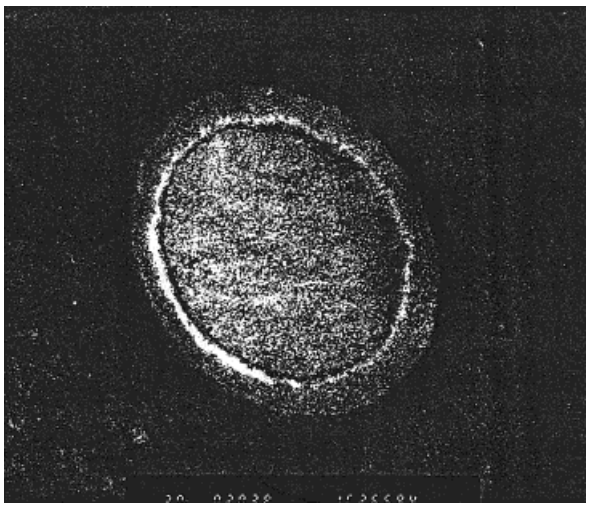

Figure 7 A TEM micrograph of an ADC particle with a circumferential region in the ADC50/UC50 SIN (original magnification ×30,000).

DMA Measurements

The temperature dependence of the loss modulus maximum for ADC/UC SINs containing 10–50% UC and pure UC component is shown in Figure 8. In order to retain the clarity in Figure 8, the loss modulus versus temperature plot of the ADC neat resin is shown separately in Figure 9. All ADC/UC SINs showed one broad peak whose maxima was between the two T_g values of the pure ADC and UC components. A single glass transition obtained from the DMA appeared to be contradictory with the TEM micrographs of the ADC/UC SINs containing 20, 30, and 50% UC, which clearly showed a two-phase morphology. This discrepancy between the DMA results and TEM micrographs may have resulted from the small difference between the two T_g values of the pure components of ADC and UC, which could not be distinguished as two distinct maxima in the DMA thermograms. However, as shown in Figure 8, the single maximum loss modulus peak moved toward the UC glass transition as the UC content increased to 30%. This was consistent with the TEM micrograph of the ADC70/UC30 SIN in which the UC phase appeared as a continuous phase. As the UC content was increased to 50%, the maximum loss modulus peak in the DMA plot surprisingly approached the ADC glass transition. This may be attributed to the dispersion of the very fine ADC particles size (i.e., the small range of the bimodal distribution) within the UC matrix phase at this composition. Hence, the higher miscibility between the UC continuous phase and the ADC dispersed phase shifted the maximum loss modulus peak toward the ADC glass transition.

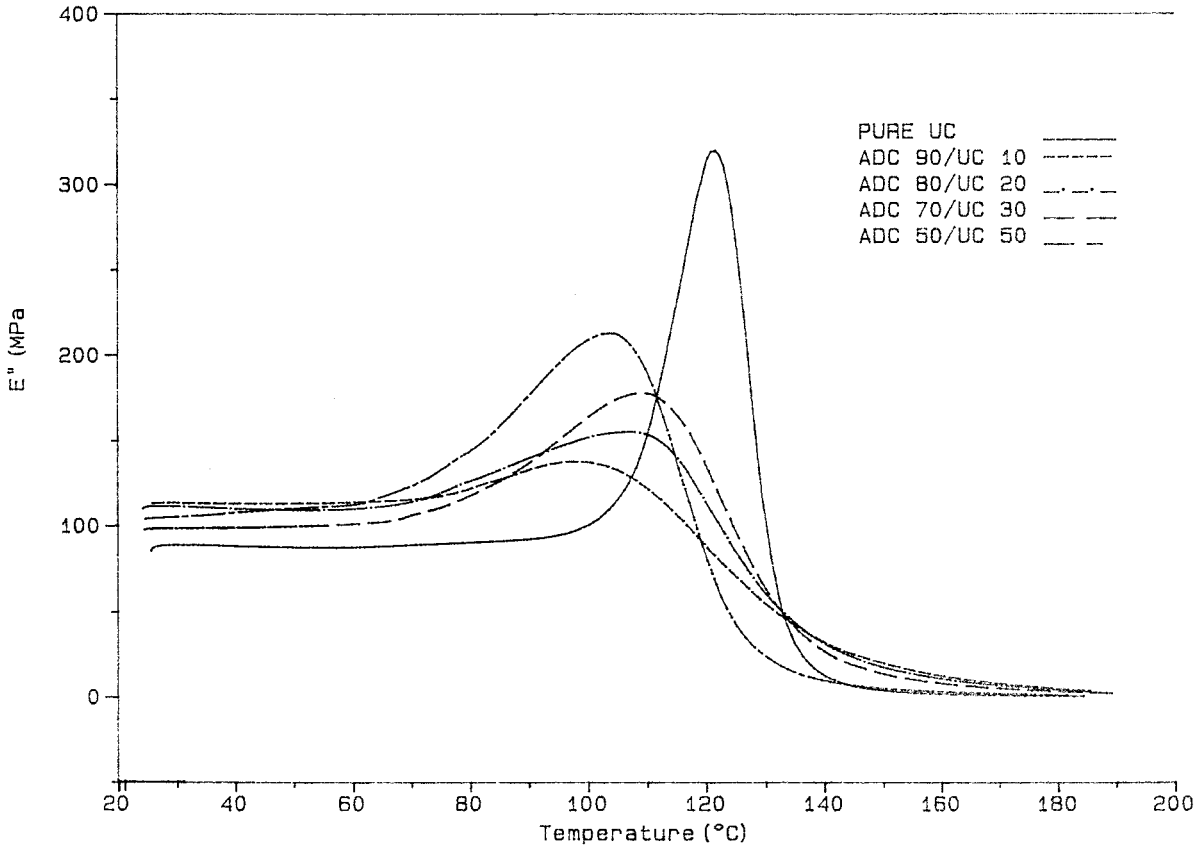

Figure 8 The variation of the loss modulus with temperature for ADC/UC SINs at different compositions.

Mechanical Properties

The modulus of the SINs (Fig. 10) up to 30% UC content remained at the level of the unmodified ADC and UC networks. The modulus then increased slightly to a higher value at a UC content of 50%. This synergism in the modulus of the ADC50/UC50 was most likely a result of the increase in crosslink density attributable to increased physical crosslinks caused by a greater degree of entanglement between the two networks (particularly at the phase boundaries). However, the tensile strength of the SINs (Fig. 11) showed a steady increase as the UC content increased.

The variation of the elongation with the UC content (Fig. 12) in the ADC/UC SINs showed very interesting and unexpected behavior. A sharp increase in elongation was observed at a composition of 50%, which was approximately 4 times that of the unmodified UC and ADC homopolymers. This sample also showed a yield point in the tensile mode that indicated the ductile characteristic of the ADC50/UC50 SIN. The reason for this significant ductile behavior was probably the strong interfacial bonding between the ADC particles and the UC matrix phase caused by interpenetration. The fracture toughness of the SINs (Fig. 13) up to 30% UC content lay between those of the two constituent networks. As the UC content was raised to 50%, the fracture toughness was moderately increased.

Fracture Surfaces

The fracture surface of the unmodified UC showed fine crack ridges running across the fracture surface (Fig. 14) while the ADC resin exhibited a featureless fracture surface (Fig. 15). The SIN with 10% UC content showed relatively ductile features on the fracture surface (Fig. 16), which was consistent with the 30% increase in K_{1c} over the unmodified ADC resin. The fracture surface of the ADC80/UC20 SIN studied by SEM showed a two-phase morphology (Fig. 17). The UC-phase particles appeared as a dispersed phase in the continuous ADC phase as was revealed by the TEM micrograph of this sample

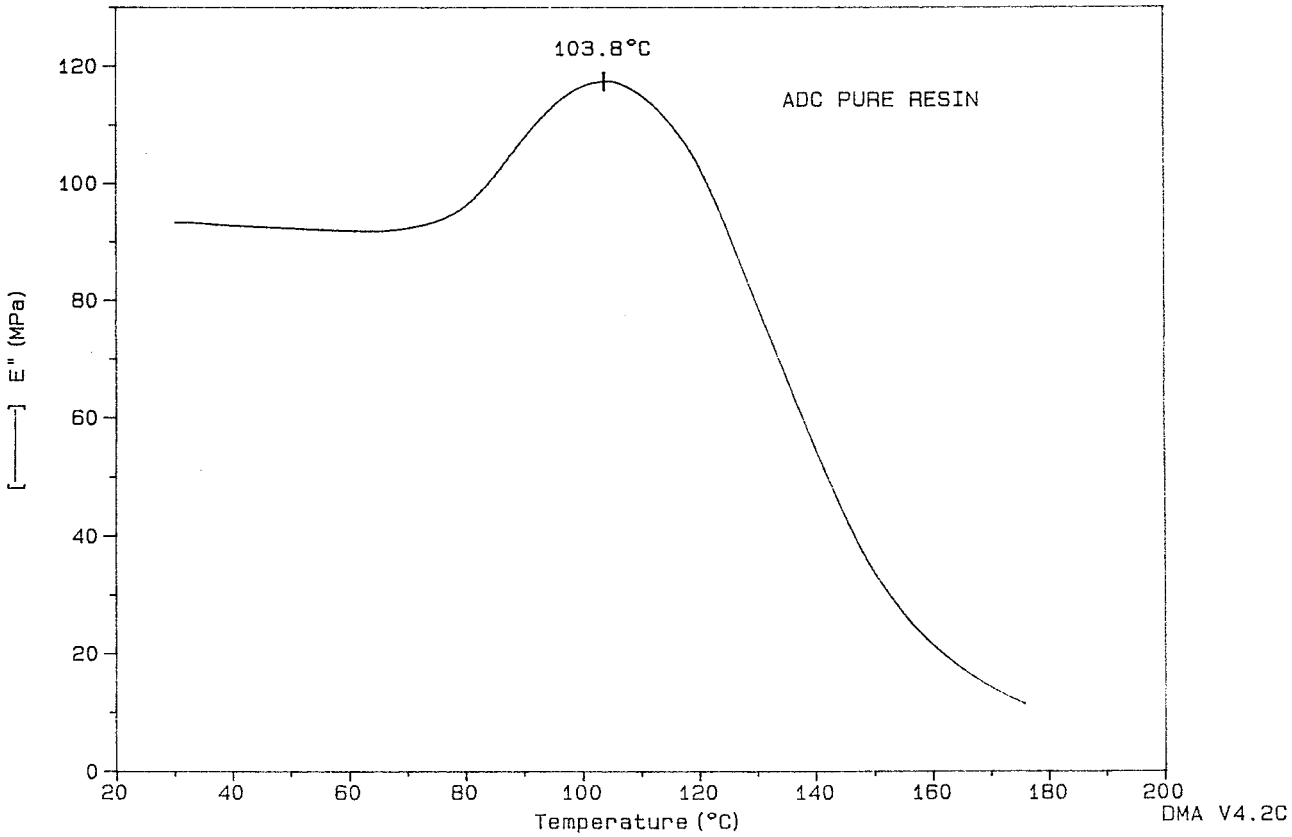

Figure 9 The variation of the loss modulus of the ADC homopolymer with temperature.

(Fig. 3). As shown in Figure 17, the fracture surface exhibited a rougher surface than the single-phase 10% SIN, suggesting more energy dissipation during the fracture process. It appeared that crack pinning also occurred with the UC particles; however, the increase in toughness was only slightly higher than 10% SIN. Thus, the UC particles did little to induce extensive shear yielding in the highly crosslinked ADC matrix. This result was in agreement with the result reported by other researchers[22–24] on highly crosslinked ther-

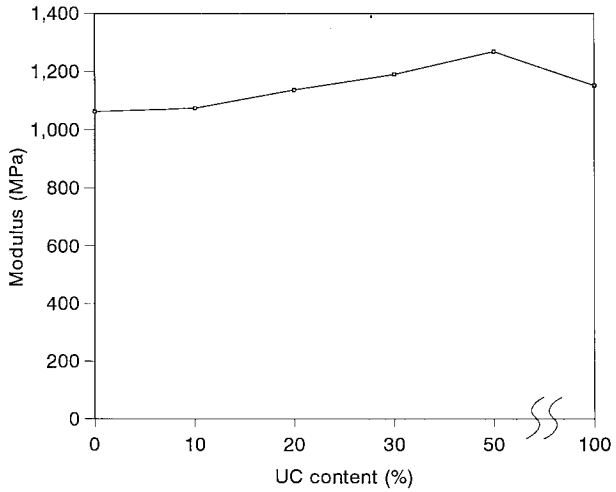

Figure 10 The variation of the modulus of the ADC/UC SINs with composition.

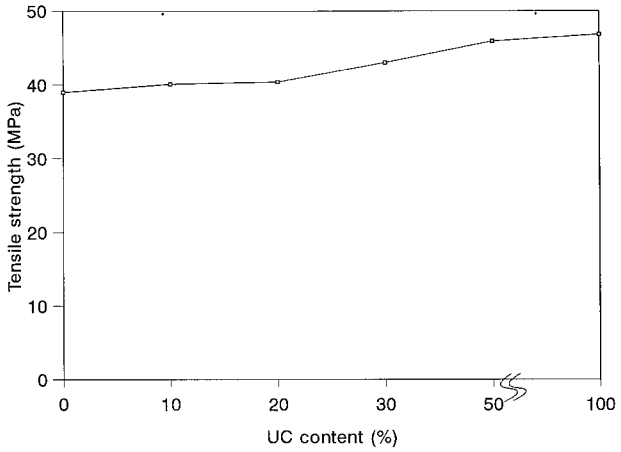

Figure 11 The variation of the tensile strength of the ADC/UC SINs with composition.

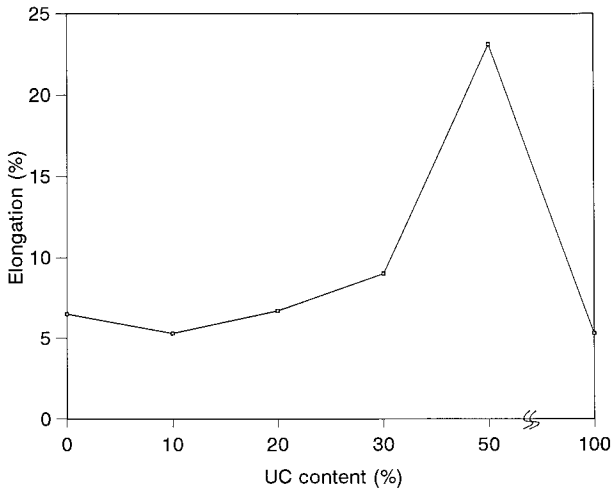

Figure 12 The variation of the elongation of the ADC/UC SINs with composition.

moset resins in which the discrete particles were not effective enough to induce sufficient plastic deformation in the thermoset matrix.

The fracture surface of the SIN with 30% UC content also exhibited a two-phase morphology as shown in Figure 18. In addition, comparing the SEM micrograph of the ADC70/UC30 SIN with its corresponding TEM micrograph (Fig. 4) revealed that in this morphology the spherical ADC particles were embedded in the continuous UC phase. The particle–matrix interfacial bonding appeared to be strong because there was no indication of debonding. The matrix showed ductile features but the fracture toughness of the SIN (k_{1c} = 1.03) was lower than unmodified UC (k_{1c} = 1.54). The crack-pinning features were not

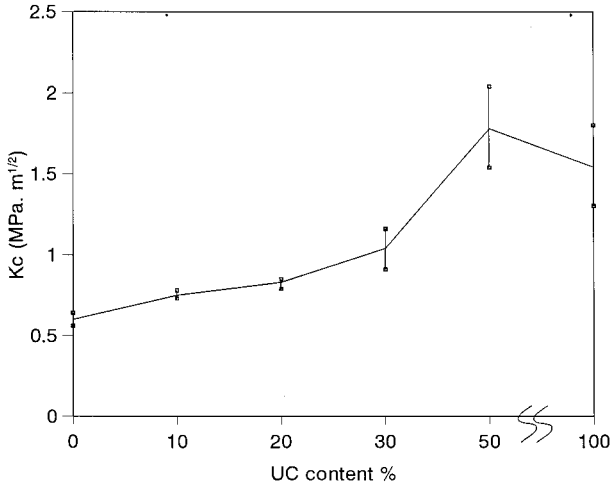

Figure 13 The variation of the fracture toughness (k_{1c}) of the ADC/UC SINs with composition.

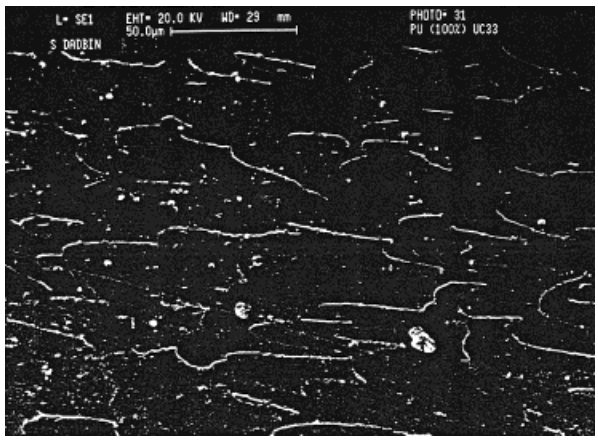

Figure 14 The SEM fracture surface of the pure UC network (original magnification ×500).

present on the fracture surface. Thus, the rigid, rather large ADC particles in the UC matrix did not contribute to the fracture toughness by either shear yielding or other less effective mechanisms such as crack pinning.

The fracture surface of the ADC50/UC50 SIN exhibited debonding between the matrix and the large ADC particles as shown in Figure 19. The voids appeared to be larger than the ADC particles residing inside (Fig. 20). Hence, the increase in toughness of this SIN (k_{1c} = 1.77 MPa $m^{1/2}$) over the unmodified UC (k_{1c} = 1.54 MPa $m^{1/2}$) may have been related to the debonding of the ADC particles from the UC matrix, which enabled the growth of plastic voids in the matrix as was suggested by Huang et al.[22] for toughened epoxy systems. Plastic energy was dissipated during this plastic flow process, which contributed to the

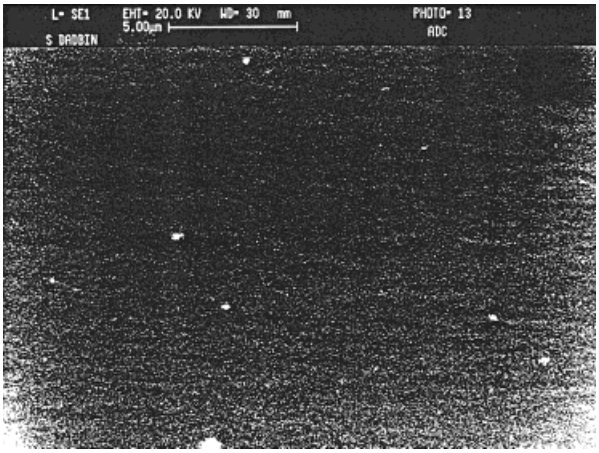

Figure 15 The SEM fracture surface of the ADC network (original magnification ×5000).

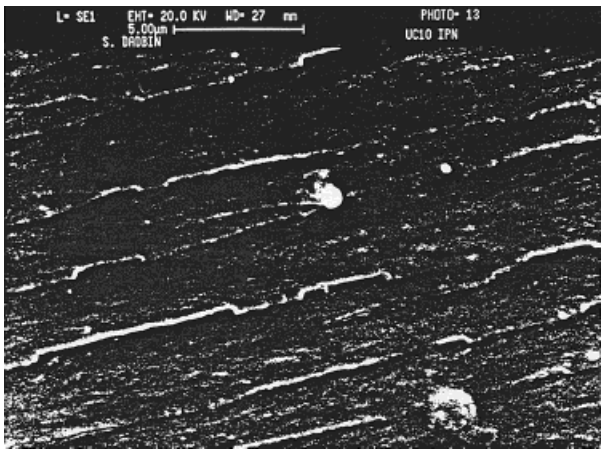

Figure 16 The SEM fracture surface of the ADC90/UC10 SIN (original magnification ×5000).

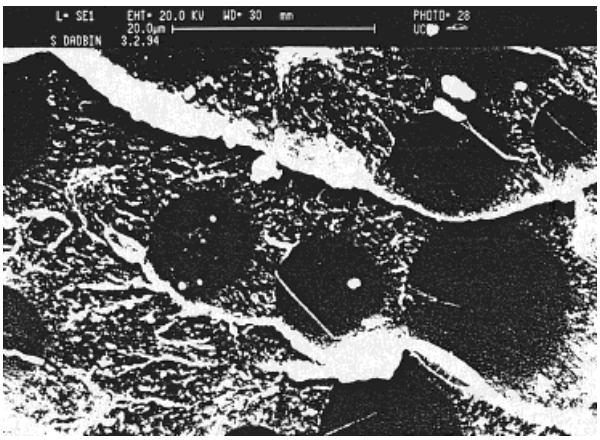

Figure 18 The SEM fracture surface of the ADC70/UC30 SIN (original magnification ×2000).

toughness of the material. The higher toughness of this sample also suggested that the debonding occurred at very high loading in the vicinity of the matrix yield stress. According to Huang et al.,[22] the debonding process was only effective if it occurred close to the yield point of the matrix. Thus, there should be strong interfacial bonding between the particles and matrix. Indeed, if debonding occurred from the first instant of loading (i.e., when the material was far from local plastic deformation), voiding could only be damaging.

CONCLUSION

SINs of ADC and Conathane UC-33, which is a rigid polyurethane prepolymer system, were synthesized. We found that the morphology was remarkably influenced by the composition of the SINs. A one-phase morphology accompanied by excellent optical transparency was obtained in the SIN containing 10% UC while a two-phase morphology with some loss of transparency was observed as the UC content increased. In spite of the two-phase morphology of the SINs containing 20, 30, and 50% UC, the loss modulus plots versus the temperature exhibited a broad peak with a single maximum between the glass transitions of the two constituent components.

The mechanical properties of the SINs were influenced by the morphology of the SINs. It was shown that only moderate improvement of the fracture toughness was achieved in the two-phase SINs where the UC particles were dispersed in the ADC matrix. As the UC network became the matrix phase in the ADC/UC SINs, synergistic

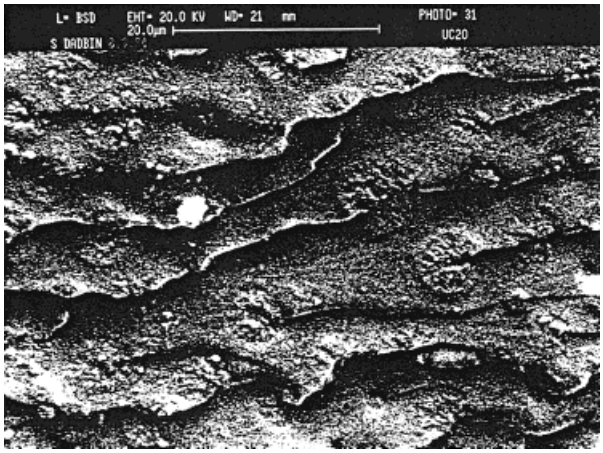

Figure 17 The SEM fracture surface of the ADC80/UC20 SIN (original magnification ×2000).

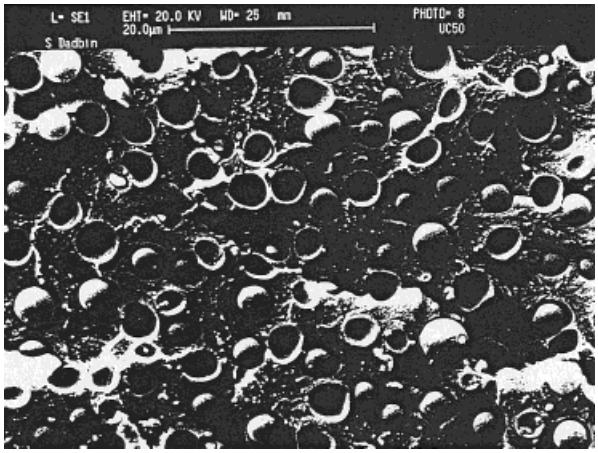

Figure 19 The SEM fracture surface of the ADC50/UC50 SIN (original magnification ×2000).

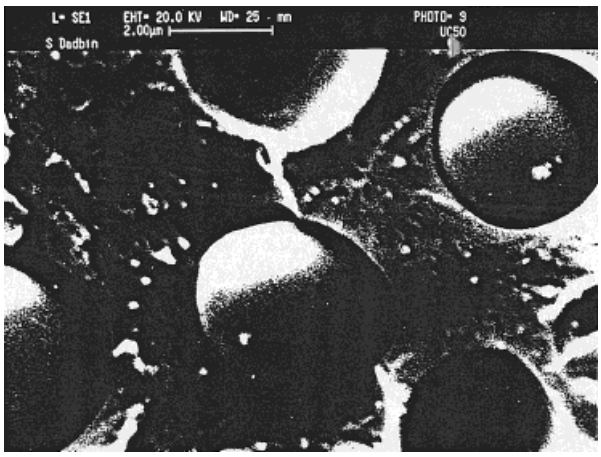

Figure 20 The SEM fracture surface of the ADC50/UC50 SIN (original magnification ×10,000).

mechanical properties were observed at the midrange composition. The elongation at break was increased 4 times that of the unmodified constituent components. The fracture toughness was considerably enhanced over the neat ADC but only moderately over the neat UC. The modulus and tensile strength were also moderately increased.

REFERENCES

1. Sperling, L. H. Polymeric Multicomponent Materials; Wiley: New York, 1997; Chap. 10.
2. Sperling, L. H. Interpenetrating Polymer Networks and Related Materials, Plenum: New York, 1981.
3. Sperling, L. H. In Multicomponent Polymer Materials; Paul, D. R., Sperling, L. H., Eds.; Advances in Chemistry Series 211; American Chemical Society: Washington, DC, 1986.
4. Park, I. H.; Lee, J. H.; Kim, S. C. Polym Bull 1983, 10, 126.
5. Lee, D. S.; Kim, S. C. Macromolecules 1984, 17, 268.
6. Frisch, H. L.; Zhou, P. In Interpenetrating Polymer Networks; Klempner, D., Sperling, L. H., Utracki, L. A., Eds.; Advances in Chemistry Series 239; American Chemical Society: Washington, DC, 1994.
7. Zhou, P.; Frisch, H. L.; Ghiradella, H. J Polym Sci A 1992, 30, 835.
8. Frisch, H. L.; Frisch, K. C.; Klempner, D. Pure Appl Chem 1981, 53, 1557.
9. Tabaka, M. T.; Widmaier, J. M.; Meyer, G. C. In Sound and Vibration Damping with Polymers; Corsaro, R. D., Sperling, L. H., Eds.; ACS Symposium Series 424; American Chemical Society, Washington, DC, 1990.
10. Dadbin, S.; Burford, R. P.; Chaplin, R. P. Polym Gels Networks 1995, 3, 179.
11. Dadbin, S.; Burford, R. P.; Chaplin, R. P. Polymer 1996, 37, 785.
12. Xue, Y.; Frisch, H. L. J Polym Sci A 1994, 32, 257.
13. Hourston, D. G.; McCluskey, J. A. J Appl Polym Sci 1986, 31, 645.
14. Edbon, R. J.; Hourston, D. J.; Klein, P. G. Polymer 1984, 25, 163.
15. Fox, R. B.; Fay, J. J.; Sorathia, U.; Sperling, L. H. In Sound and Vibration Damping with Polymers; Corsaro, R. D., Sperling, L. H., Eds.; ACS Symposium Series 424; American Chemical Society: Washington, DC, 1990; p 359.
16. Touhsaent, R. E.; Thomas, D. A.; Sperling, L. H. In Toughness and Brittleness of Plastics; Deanin, R. D., Crugnola, A. M., Eds.; Advances in Chemistry Series 154; American Chemical Society, Washington, DC, 1976; p 206.
17. Frounchi, M.; Burford, R. P.; Chaplin, R. P. Polymer 1994, 35, 5073.
18. Frounchi, M.; Westgate, T. A.; Chaplin, R. P.; Burford, R. P. Polymer 1994, 35, 5041.
19. Morin, A.; Djomo, H.; Meyer, G. C. Polym Eng Sci 1983, 23, 394.
20. Hermant, U.; Damyanidu, M.; Meyer, G. C. Polymer 1983, 24, 1419.
21. Brown, W. F.; Strawley, J. E. ASTM Special Technical Publication 410; American Society for Testing and Materials: Philadelphia, PA, 1986.
22. Huang, Y.; Hunston, D. L.; Kinloch, A. J.; Riew, C. K. In Toughened Plastics 1; Riew, C. K., Kinloch, A. J., Eds.; Advances in Chemistry Series 233; American Chemical Society: Washington, DC, 1993; p 20.
23. Pearson, R. A.; Yee, A. F. J Mater Sci 1989, 24, 2571.
24. Hwang, J. F.; Manson, J. A.; Hertzberg, R. W.; Miller, G. A.; Sperling, L. H. Polym Eng Sci 1989, 29, 1466.